ELSEVIER

Catalysis Today 36 (1997) 227–241

CATALYSIS TODAY

Molybdenum catalyzed carbonylation of ethylene to propionic acid and anhydride

Joseph R. Zoeller*, Elizabeth M. Blakely, Regina M. Moncier, Todd J. Dickson

Eastman Chemical Company Research Laboratories, Kingsport, TN 37662, USA

Abstract

We have discovered a low pressure and low temperature process for the single step conversion of ethylene and carbon monoxide to either propionic acid or anhydride utilizing surprisingly active, inexpensive Cr group based catalysts which operate at very high rates under low-to-moderate pressures (30–70 atm) and temperatures (150–200°C). Mechanistic investigations of the Mo based process, which is clearly the most active metal of the group, imply that catalysis is initiated by a rate limiting CO dissociation from $Mo(CO)_6$. This dissociation appears to be followed by a process which ultimately transfers an I atom from *Et*I to the coordinatively unsaturated $Mo(CO)_5$, probably via an inner sphere, electron transfer process. Subsequent reaction of the resultant ethyl radical with $Mo(CO)_6$ probably generates very reactive odd electron Mo species which are capable of rapid catalysis via classical olefin carbonylation mechanisms. This discovery represents the first case of an efficient carbonylation process based on the Cr group metals and a unique method for initiating carbonylation catalysis. A general description of this process and the mechanistic proposal, which is based on detailed kinetics, spectroscopy and model reactions, will be presented.

Keywords: Molybdenum; Carbonylation; Reaction kinetics; Spectroscopy; Model reaction

1. Introduction

Propionic acid and its derivatives represent an important and rapidly growing class of chemical intermediates, with applications ranging from food and grain preservatives to the generation of propionate esters, such as cellulose propionate based plastics. As the chemical industry is seeking a combination of safer, more environmentally benign processes and products, along with better product performances, the potential of propionate derivatives as feedstocks, particularly for the generation of methacrylic acid derivatives and higher performance ester derivatives, continues to rise rapidly. To realize this potential, improved processes for the generation of these materials will be required.

In principle, hydrocarboxylation (or hydroesterification in the case of esters), which is depicted in Eq. (1), represents the most direct process for the generation of these intermediates and is capable of generating any of the usual derivatives in a single step. Although these processes are well known [1], commercial application has been limited to a single unit at BASF which uses a highly toxic (and very volatile) $Ni(CO)_4$ catalyst operating at high pressures (>180 atm) and high temperatures (>270°C) [1,2] to produce

*Corresponding author.

PII S0920-5861(96)00222-2

propionic acid. Alternative catalysts which may operate at substantially lower pressures and temperatures generally require expensive catalysts such as Rh, Ir, or Pd and none have been employed commercially [2–6]. Given the harsh conditions and the expense associated with the alternative catalysts, most current producers of propionate derivatives still proceed through the more circuitous hydroformylation-oxidation sequence to generate propionic acid, which is subsequently converted to its derivatives in a separate step.

$$H_2C{=}CH_2 + CO{+}ROH \rightarrow EtCO_2R \quad (1)$$

R = H, EtC=(O), alkyl (Me, Et, etc.)

While seeking improved processes for the propionates, we discovered that halide promoted Cr group (Group 6) metals, preferably in the form of an iodide promoted Mo catalyst, allowed the carbonylation of olefins to carboxylic acid derivatives to proceed at low to moderate pressure (25–70 atm) and moderate temperatures (150–200°C) with very high rates. With the proper application of the catalyst system described in this report, we have found that the carbonylation of ethylene to propionate derivatives can be operated up to the limits imposed by mass transfer of the reactant gases, and that Mo turnovers of >150 h^{-1} are readily achievable.

Although Cr group metals have been reported in numerous instances to act as 'promoters' or 'stabilizers' when used in combination with known carbonylation catalysts, such as Co, Ni, Rh and Ir, they have never been shown (or believed) to have significant catalytic activity in isolation. In fact, prior to this study, the only known examples where Cr group metals have been demonstrated to induce carbonylation in any substrate were limited to a stoichiometric carbonylation of alkyl iodides to esters using a $Mo(CO)_6/F^-$ catalyst [7] and a marginally catalytic (approx. 0.6 turnovers h^{-1}) carbonylation of α-difluorinated iodides using $Mo(CO)_6$ [8]. Therefore, the process described in this report represents the first demonstration of an efficient carbonylation catalyst utilizing a Cr group metal as the catalytically active metal component. Within this communication, we will describe the key characteristics of this process, a detailed study of the Mo catalyzed generation of propionic anhydride, and provide a detailed mechanistic interpretation.

2. Experimental

2.1. General procedure for the generation of propionic anhydride [$(EtCO)_2O$]

To allow the measurement of rates, a 2-liter Hastelloy® C overhead stirred autoclave was fitted with a high pressure condenser and a dip tube for removing samples during the course of the reaction. Gas mixtures were prepared in a stirred gas mix tank heated to 45–50°C and feed lines were heat traced and maintained at 40–50°C. Failure to keep the mix tank and lines heated often leads to ethylene liquefaction and separation, particularly when cooling begins to occur (due to expansion) as ethylene is either added to the tank during preparation of the gas mixture or is removed from the tank during the reaction. The following procedure is exemplary of a typical operation.

To the autoclave, 5.81 g (0.022 mol) $Mo(CO)_6$, 15.5 g (0.040 mol) tetrabutylphosphonium iodide, 109.2 g (0.700 mol) ethyl iodide and 555 g (7.5 mol) propionic acid were added. The condenser temperature was set at 5–10°C using a cooled ethylene glycol/water mixture. The autoclave was then pressure tested with nitrogen at 68.0 atm and a gas purge of 3 mol h^{-1} of gas was established through the high pressure condenser (during the reaction this gas purge permitted control of the gas composition over the reaction mixture and is necessary for kinetic measurements). The nitrogen was vented, the autoclave was then pressurized to 23.8 atm with 5% hydrogen in carbon monoxide, and subsequently heated to 160°C (the 3 mol h^{-1} of gas purge is maintained throughout heating and the subsequent reaction). Upon reaching temperature, the pressure is raised to 51.0 atm using a gas mixture consisting of 6% H_2, 47% CO and 47% ethylene while using the 3 mol h^{-1} purge to maintain the gas mixture. Liquid samples were removed every 20 min for 5 h and analyzed for ethyl iodide, ethyl propionate, propionic anhydride and propionic acid content by GC using a Hewlett–Packard 5890 GC containing a 25 m (0.25 mm ID, 0.25μ film) Quadrex 007 FFAP Capillary Column with p-xylene as an internal standard. (A split injection was used to introduce the sample; sample detection was accomplished with a TCD detector.) These components represented the only significant products and all other materials detectable by GC–MS were present at trace levels. Gas samples

were also removed hourly and analyzed by GC to ensure that the gas mixture is consistent. The molar quantities of propionic anhydride (n_{pan}) formed were determined from the GC data using the following equation:

$$n_{pan} = \frac{X_{pan}}{130} \times \frac{n^0_{pa} + n^0_{ei}}{[(X_{ei}/156) + (X_{pa}/74) + (X_{pan}/130) + (X_{ep}/102)]}$$

where

n_i =moles of the component

X_i =weight fraction of the component (obtained from GC analysis)

n^0_{pa} =moles of propionyl initially present, = propionic acid added at start

n^0_{ei} =ethyl iodide initially added

Subscript designations:

ep =ethyl propionate

pa =propionic acid

pan =propionic anhydride

ei =ethyl iodide

The molar quantities were plotted against time and the reaction displayed an essentially linear behavior from approx. 20 min into the reaction until the conversion of propionic acid approached approx. 65–70% when the effects of dilution start to become apparent (the 20-min 'lag' is not due to an 'initiation' period, but represents the time it takes to replace the H_2/CO gas mix within the autoclave with the reaction mixture of ethylene/CO/H_2). Therefore, the rate of the reaction (expressed as moles of propionic anhydride formed kg^{-1} of initial reaction solution h^{-1}) was easily determined by using a best fit slope of this plot until either the 5 h reaction period had expired or the conversion reached 65%. Using this method, the rate of propionic anhydride formation was determined to be 1.39 mol kg^{-1} h^{-1} (181 g (kg initial solution)$^{-1}$ h^{-1}). Experimental reaction orders for different components were readily determined from plots of rate as a function of each gas and catalyst component at varying levels using standard regression methods.

This apparatus and procedure readily allow access to studies on the effect of different gas components by changes in the gas composition. The use of a purged system allows us to maintain consistent gas compositions above the reactor regardless of stoichiometry or a bias in the gas absorbed. Using conditions which displayed very high rates, the reactor system was tested for mass transfer limitations by adjusting the stirring rate of the autoclave. It was found that, with this equipment, mass transfer (gas dissolution) limitations typically began to be observable when rates exceeded 4 mol kg^{-1} h^{-1}, representing 8 mol of gas absorbed kg^{-1} solution h^{-1}. Therefore, all our chemical kinetic measurements in this report have been limited to reactions not exceeding 3.5 mol kg^{-1} h^{-1} to avoid introducing mass transfer complications.

2.2. *General procedure for the generation of propionic acid [EtCOOH]*

The same apparatus and general procedure were used for the generation of propionic acid as for the generation of propionic anhydride, except that the process was run at 190°C and the propionic acid was replaced with a mixture of 81 g (4.5 mol) H_2O and 450 g (7.5 mol) acetic acid (AcOH) (the AcOH is present as both solvent and internal standard). The liquid samples obtained were analyzed for ethyl acetate, ethyl propionate, acetic acid, and propionic acid by GC (the analysis uses the same GC, GC column, and internal standard as the propionic anhydride process). Molar quantities of propionyl units generated were calculated by the following equation:

$$n_p = \frac{[(X_{pa}/74) + (X_{ep}/102)] \cdot n^0_a}{[(X_{ea}/88) + (X_{aa}/60)]} \quad (3)$$

where

n =moles

X =weight fraction (obtained from GC analysis)

n_p =total moles of propionyl products= $\sum$ propionic acid+ethyl propionate

n_a^0 =moles of acetyl initially present= acetic acid added at the start

Subscript designations:

ep =ethyl propionate

pa =propionic acid

ea =ethyl acetate

aa =acetic acid

3. Results and discussion

3.1. General description of the catalyst

Outside of the obvious requirement for the ethylene and CO reactants, the catalyst system requires the presence of a Group 6 metal, a halide salt, and an organic halide (obviously, materials which generate the organic halide or the halide salt in situ may be used as well). Ratios of the components are not critical, although each component enters the rate equation. As displayed in Table 1, the observed order of reactivity for the Group 6 metal component is Mo≫W>Cr and the halide employed may be either Br or I (presumably, the chloride would also be useful, but the volatility and toxicity of *Et*Cl precluded it from our investigation). The metal catalyst should be added as $Mo(CO)_6$ which is a readily available, inexpensive and easily handled (albeit highly toxic) solid (the only other low cost source of Mo, namely, the Mo oxides, do not readily generate active catalysts). Choice of the cationic component of the salt is important and will be discussed in detail later in this report.

The CO partial pressure and temperature are critical parameters. As we will describe later in the detailed kinetic discussion, the catalyst system operates most rapidly at the lowest pressures consistent with catalyst stability and adequate mass transfer of the gas components. At 160°C, the apparent minimum CO partial pressure is around 10–15 atm in our equipment. Lower pressures lead to loss of catalyst activity and higher pressures are required as the temperature is elevated. We have also found it useful to include a portion of H_2 in the process. The addition of H_2 both accelerates the initial reaction rate and maintains the reaction rate. In the absence of extraneously added H_2, the initial reaction rate is ca. 30% slower and becomes increasingly sluggish as time proceeds. However, it is important to indicate that in the absence of intentionally added H_2, the reaction generates significant amounts of H_2 spontaneously.

For reasons we will elucidate later, the behavior of the catalyst is quite different as we alter the nucleophilic component of the process. As displayed in Fig. 1, a typical Mo catalyzed process in which we add propionic acid to generate propionic anhydride (i.e., *R*=*Et*CO in Eq. (1)) yields a clean, nearly linear production of propionic anhydride over a large span of time. However, when water is substituted as the primary nucleophile (*R*=H in Eq. (1)), the reaction is initially very sluggish, but accelerates as the reaction proceeds (similar observations are made if methanol is added to generate methyl propionate).

Further, the catalyst is not readily applicable to the carbonylation of non-olefinic substrates. For example, attempted carbonylations of methanol, methyl acetate, benzyl alcohol, and benzyl acetate all proceed very sluggishly, if at all, under even the best of conditions

Table 1
Comparison of different halides and Group 6 metal hexacarbonyl catalysts for the carbonylation of ethylene to propionic anhydride [a]

Metal carbonyl	Halide	Bu_4P^+ salt (mmol)	Rate	Turnover No.
$Mo(CO)^6$	I	40	1.39	41
$Mo(CO)^6$	Br	40	1.04	31
$Mo(CO)^6$	I	72	2.22	71
$Cr(CO)^6$	I	72	0.18	6
$W(CO)^6$	I	72	0.14	5

[a] Conditions: Metal hexacarbonyl, 22 mmol; *EtX* (*X*=halide), 0.7 mol; *Et*COOH, 7.5 mol; Bu_4PX, quantity as indicated; temperature, 160°C; pressure, 55 atm. Gas composition: 5% H_2, 45% C_2H_4, 50% CO. Rate: mol $(EtCO)_2O$ (kg initial solution)$^{-1}$ h^{-1}; and Turnover No.: mol $(EtCO)_2O$ (mol metal carbonyl)$^{-1}$ h^{-1}.

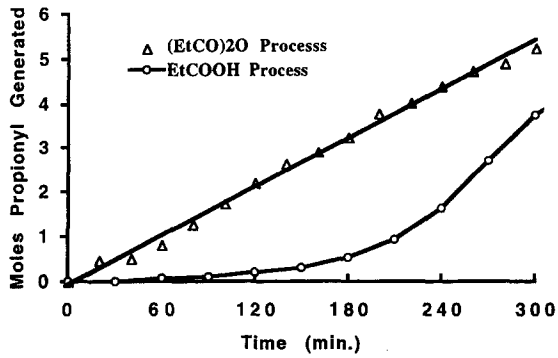

Fig. 1. Comparison of Mo catalyzed processes for propionic acid and propionic anhydride. Catalyst composition: *Et*I, 0.7 mol; $Mo(CO)_6$, 22 mmol; Bu_4PI, 40 mmol. Gas composition: 5% H_2, 50% C_2H_4, 45% CO; pressure, 55 atm; Temperature/reactants/solvent: (a) propionic acid (*Et*COOH) process: 190°C/H_2O, 4.5 mol/AcOH, 7.5 mol (solvent); and (b) propionic anhydride ($(EtCO)_2O$) process: 160°C/*Et*COOH, 7.5 mol/(no solvent).

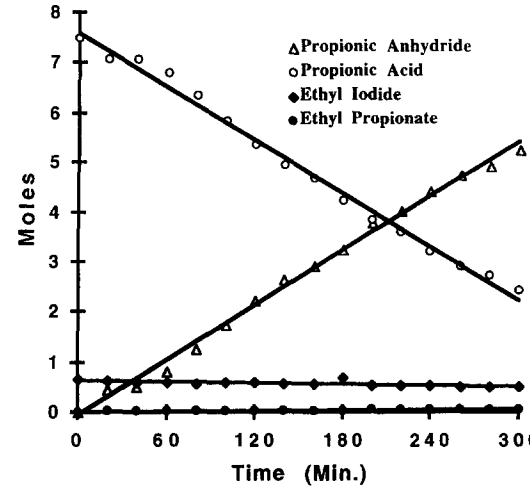

Fig. 2. Reaction profile for the carbonylation of ethylene to propionic anhydride. Initial composition: *Et*I, 0.7 mol; *Et*COOH, 7.5 mol; $Mo(CO)_6$, 22 mmol; Bu_4PI, 40 mmol. Conditions: 160°C, 55 atm. Gas composition: 5% H_2, 50% C_2H_4, 45% CO.

for these catalysts. Olefins other than ethylene undergo carbonylation but proceed at slower rates yielding a mixture of carboxylic acid isomers.

The unique nature of this catalyst system and the peculiar behavior as the nucleophiles were altered prompted us to undertake a detailed study of the Mo catalyzed process. This study focused on the propionic anhydride process due to its simple kinetic behavior.

3.2. *Detailed study of the Mo catalyzed carbonylation of ethylene to propionic anhydride*

When the process is operated with a catalyst composed of Bu_4PI, $Mo(CO)_6$, and *Et*I the Mo catalyzed carbonylation of ethylene to propionic anhydride proceeds smoothly, with a near linear generation rate, until a 75–85% conversion of the propionic acid is achieved at which point the reaction begins to slow markedly. A typical reaction profile for this process appears in Fig. 2. The ultimate reaction rates attainable in this process were limited not by catalyst performance, but by mass transfer of the gaseous reactants into the reaction medium. The following observations are important in reaching a mechanistic understanding of this unique process, and in anticipation of a mechanistic proposal we have noted the significant (or potentially significant) implications of each observation.

3.2.1. *By-products*

The main by-product in this process is ethyl propionate, probably generated by the acid catalyzed addition of propionic acid to ethylene or nucleophilic displacement of iodide from ethyl iodide. It is generally around 1% of the reaction mixture, never exceeds 2% of the product mixture, often decreases as the conversion rises, and is a possible substrate for further derivatization to propionic anhydride. More informative is the identification of trace by-products. In the Bu_4PI-$Mo(CO)_6$-*Et*I catalyzed system, we observe traces of (1) 3-oxo-4-hexyl propionate, (2) 3-oxo-4-hexenyl propionate, (3) 5-ethyl-2-oxo-1,5-dihydrofuran and (4) 1,1-propyl dipropionate in the GC–MS. Compounds 1 and 2 were probably derived via known chemistry from 3,4-hexane dione [9], the coupling product of propionyl radicals. This provided our first hint to pursue the possibility of a radical pathway (compound 3 is probably formed by a second sequential ethylene and CO insertion into a Mo–C(=O)*Et* moiety). One key observation is that we have yet to detect any diethyl ketone or ethane in the process.

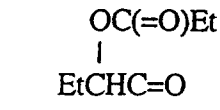

1

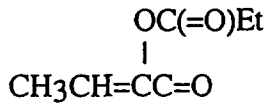

2

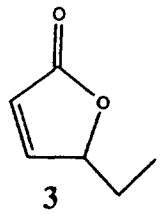

3

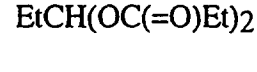

4

Table 2
Comparison of various salts or potential salt precursors for the carbonylation of ethylene to propionic anhydride [a]

Entry No.	Salt or Group 15 promotor	Rate
1	Bu_4PI	1.39
2	Et_4PI	1.51
3	Ph_4PI	1.95
4	Bu_4NI	1.05
5	NaI	0.79
6	KI	0.66
7	CsI	0.15
8	Ph_3P	2.20
9	Ph_3As	0.03
10	Ph_3N	0.18
11	Pyridine	2.20
12	4-Methyl imidazole	1.52
13	2,2′-Dipyridyl	0.13
14	$(n\text{-}C_8H_{15})_3P$	2.20
15	$(n\text{-}C_8H_{15})_3P{=}O$	0.20
16	$Ph_3P{=}O$	0.09
17	Bu_3P	2.20
18	$(\text{cyclo-}C_6H_{11})_3P$	2.49
19	$Ph_2P(CH_2)_2PPh_2$	1.18
20	$Ph_2P(CH_2)_3PPh_2$	1.23
21	$Ph_2P(CH_2)_4PPh_2$	1.48
22	$Ph_2P(CH_2)_5PPh_2$	1.46

[a] Conditions: $Mo(CO)_6$, 22 mmol; *Et*I, 0.7 mol; *Et*COOH, 7.5 mol; temperature, 160°C; pressure, 55 atm. Salt or Group 15 promotor, 40 mmol for entries 1–18, 20 mmol for entries 19–22 (an additional 40 mmol *Et*I added for non-alkylated materials in entries 8–22). Gas composition: 5% H_2, 45% C_2H_4, 50% CO. Rate: mol $(EtCO)_2O$ (kg initial solution)$^{-1}$ h^{-1}.

3.2.2. *The effect of the nature of cation and halide*

The nature of the cation incorporated in the salt component is important and incompletely understood. We tested a variety of materials to fit this role and the extent of these differences is evident from Table 2 (omitted from Table 2 is an entry for LiI which gave an initial burst of a small quantity of product but was incapable of sustaining the reaction for even an hour. Therefore, rates were not readily attainable with this salt). It was initially presumed that the phosphines and amines in this study underwent alkylation by reaction with ethyl iodide to form the corresponding quaternary salt. Subsequent ^1H-, ^{13}C- and ^{31}P-NMR studies of the product solutions indicated that this was true for all the monophosphines while the amines were primarily protonated species. However, for the diphosphines (Entries 19–22), there is no evidence of a diagnostic ethyl group bound to phosphorous, except in the case of 1,5-bis-diphenylphosphino-pentane (Entry 22).

There is a marked bias toward salts based on N and P (added either as the salt or generated in situ) and the possibility that there was some free phosphine or amine ligand present which altered Mo activity had to be considered. However, in the above-mentioned NMR studies, we saw no exchange of alkyl groups (ethyl for butyl) or free phosphine when Bu_4PI was used (Entry 1). Further, we saw no direct evidence of a ligated Mo carbonyl species in the in-situ infrared studies discussed in the next section. Therefore, despite the attractiveness of this hypothesis, there is presently no evidence to support a Mo species with either an N or P based ligand, at least when using the monodentate precursors.

As indicated earlier in Table 1, substitution of bromine for iodine only leads to a small change (an approx. 25% decrease) in reaction rate. This relative

insensitivity to the nature of the halide is generally diagnostic of an electron transfer process [10].

3.2.3. In-situ infrared spectroscopic studies

An in-situ infrared spectroscopic study of the $Mo(CO)_6$ with a Bu_4PI salt was undertaken by observing spectra as we:

1. heated the catalyst mixture to 160°C under 7–8 atm of 5% H_2 in CO and adjusted the final pressure to 24 atm with 5% H_2 in CO;
2. added *Et*I; and
3. added ethylene (only a few spectra are attainable in this portion of the reaction as the CO is rapidly depleted upon initiating the reaction).

Using concentrations of reagents comparable to those in Entry 1 of Table 2, the spectra of a mixture $Mo(CO)_6$ and Bu_4PI maintained at 160°C and 24 atm of 5% H_2 in CO displayed a clear, strong peak at 1985–1986 cm^{-1} diagnostic of $Mo(CO)_6$ (if other peaks were present, they were difficult to discern over noise). Upon addition of *Et*I, a second, less prominent peak rapidly arises at 2017–2024 cm^{-1}, which is probably assignable to the strongest peak for $Mo(CO)_4I_3^-$ (Lit. (Nujol) 2038 (w), 2018 (vs), 1961 (s) and 1942 (s) [11,12]). Under these conditions, the peak at 2017–2024 cm^{-1} is 5–20% of the peak at 1984 cm^{-1} (in experiments in which there is no hydrogen present, the peak at 2017 cm^{-1} gradually becomes the predominant peak). A third, very weak peak appears at 1933–1937 cm^{-1} which is assignable to $Mo(CO)_5I^-$ [13,14].

To enhance the signal-to-noise ratio for the weaker bands, the process was repeated using 2 and 3 times, respectively, the $Mo(CO)_6$ and Bu_4PI components. Under these conditions, the peak at 1933–1937 cm^{-1}, assignable to $Mo(CO)_5I^-$, becomes more prominent and a peak at approx. 2065 cm^{-1} (corresponding to one of the weaker bands for $Mo(CO)_5I^-$) becomes observable. At the extreme concentrations, very weak bands at 2007, 2024 and 2001 cm^{-1} could also be discerned upon the addition of *Et*I and ethylene which might correspond to a fourth unidentified component.

Based on a study of the relative ratios of the key peaks at 1985 and 1934 cm^{-1} as a function of pressure using high levels of $Mo(CO)_6$ and Bu_4PI (and in the absence of *Et*I), the equilibrium constant for the reaction:

$$Mo(CO)_6 + I^- \rightleftharpoons Mo(CO)_5I^- + CO \quad (4)$$

was estimated at ca. 12 atm kg mol^{-1} at 160°C. The small equilibrium constant implies that little $Mo(CO)_5I^-$ is present under reaction conditions within the usual range of concentrations and pressures used in this study.

The same series of infrared experiments were repeated using pyridine first and then NaI in place of Bu_4PI (observations were made at both our normal reaction conditions, and using twice the normal levels of Mo and salt or salt precursor). There were no discernible differences between spectra using pyridine, NaI, or Bu_4PI.

3.2.4. Kinetic effects of catalyst components and reactants

In the propionic anhydride generation, we saw no effect on the reaction rate assignable to the level of propionic acid present until >75% of the propionic acid had been converted to propionic anhydride. This simplified the kinetic investigation and we sought to measure the effects of the gas components as the first step in the understanding of this process.

Within our process we used three gases: hydrogen, ethylene, and carbon monoxide. To measure kinetic effects, we employed a continuously gas purged autoclave equipped with a liquid sampling loop. Using this apparatus, we could vary the partial pressure of each gas independently, without regard to the 1:1 CO:ethylene stoichiometry of the reaction which would normally lead to rapid depletion of the limiting gas, and still maintain a consistent gas mixture throughout the experiment.

The effect of hydrogen and ethylene (displayed in Figs. 3 and 4, respectively) were limited. Whereas hydrogen is necessary, it is only required in a small amount and there is no kinetic effect beyond that imparted by the initial couple of atmospheres. Based on the infrared experiments described above, it is clear that the role of hydrogen is to maintain the catalyst as $Mo(CO)_6$. In its absence, Mo is oxidized gradually to $Mo(CO)_4I_3^-$. Ethylene pressures had virtually no effect on the reaction rate (experimentally measured reaction order=0.06).

However, the role of carbon monoxide pressure, displayed in Fig. 5, is much more informative. The

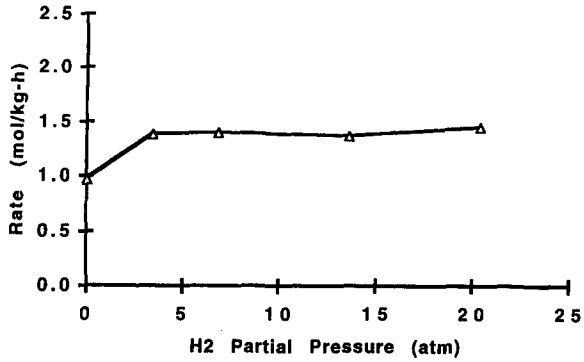

Fig. 3. Effect of hydrogen partial pressure. Initial composition: *Et*I, 0.7 mol; *Et*COOH, 7.5 mol; $Mo(CO)_6$, 22 mmol; Bu_4PI, 40 mmol. Conditions: temperature, 160°C; pressures: ethylene, 27.2 atm, CO, 23.8 atm.

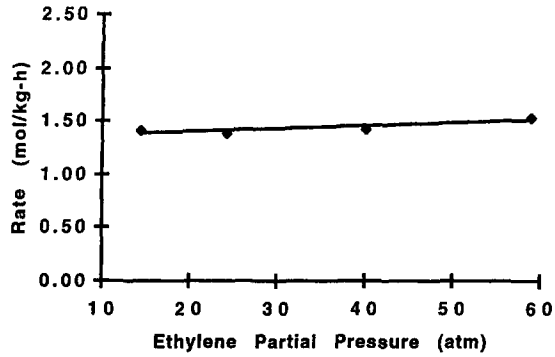

Fig. 4. Effect of ethylene partial pressure. Initial composition: *Et*I, 0.7 mol; *Et*COOH, 7.5 mol; $Mo(CO)_6$, 22 mmol; Bu_4PI, 40 mmol. Conditions: tempreature, 160°C; pressures: H_2, 3.4 atm; CO, 23.8 atm.

measured reaction order using the data in Fig. 5 was −1.17 (r^2=0.96). Given the inverse and complex (>1) order dependence upon CO pressure, it should be clear that the process must involve a step (maybe more than one, given the complex order) which is inhibited by CO.

It also implies that we should be able to operate at considerably lower pressures. Consequently, we have successfully demonstrated faster reactions at pressures as low as 15 atm of CO. However, as we attempted to go to much lower CO pressures (using 1:1 CO:ethylene feeds) the reaction rates became erratic and the activity rapidly decreased. The high pressure infrared spectroscopic experiments indicated that $Mo(CO)_6$

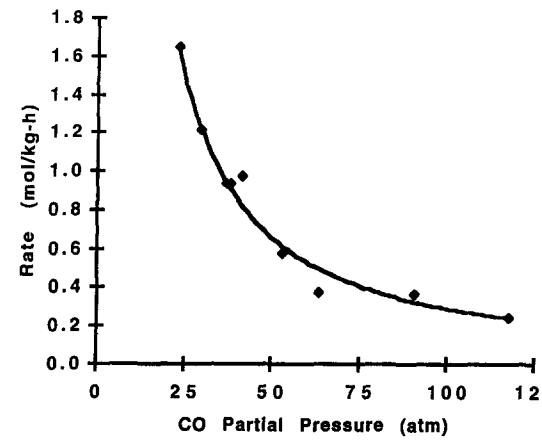

Fig. 5. Effect of CO partial pressure. Initial composition: *Et*I, 0.7 mol; *Et*COOH, 7.5 mol; $Mo(CO)_6$, 22 mmol; Bu_4PI, 40 mmol. Conditions: temprature, 160°C; pressures: ethylene, 27.2 atm; H_2, 3.4 atm.

was still stable at these lower pressures, although the amount converted to $Mo(CO)_5I^-$ rapidly rises. This conversion of $Mo(CO)_6$ to $Mo(CO)_5I^-$ and mass transfer limitations (found to be responsible for the erratic rate behavior) at these low pressures probably combine to establish the lower limit of desirable CO partial pressures at somewhere between 10–15 atm with our existing equipment.

Given the above results, we were careful to control the CO partial pressure precisely throughout the remainder of the kinetic study. To do this, we analyzed each gas mix immediately prior to use and set the CO at a constant level of 23.8 atm, ignoring any minor fluctuations in ethylene and hydrogen composition since they had little or no effect on the reaction rate. Using this approach, we studied the kinetic effect of Mo, ethyl iodide and Bu_4PI levels.

The effect of $Mo(CO)_6$ and ethyl iodide levels, which are displayed in Figs. 6 and 7, respectively, were both complex. The experimentally measured reaction order for $Mo(CO)_6$ using the data displayed in Fig. 6 was 0.62 (r^2=0.99). Whereas the experimental data for Mo was fairly consistent and gave a good experimental fit, the response to ethyl iodide was somewhat more complex. Initially determined experimental orders were 0.52, but with a somewhat mediocre statistical fit (r^2=0.92). The general form of the reaction looked more consistent with a catalyst approaching saturation. As we developed our under-

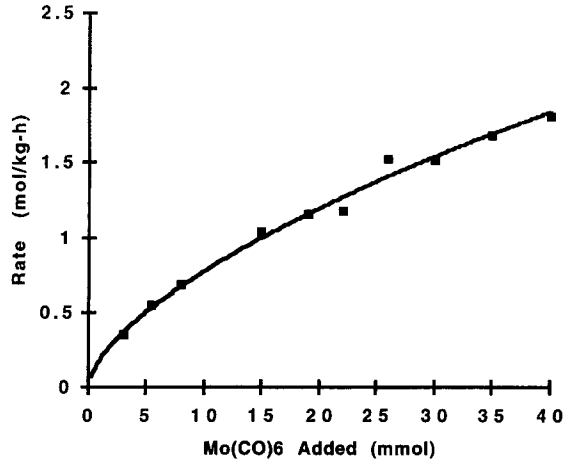

Fig. 6. Effect of $Mo(CO)_6$ levels. Initial composition: *Et*I, 0.7 mol; *Et*COOH, 7.5 mol; Bu_4PI, 40 mmol. Conditions: temperature, 160°C; pressures: ethylene, 27.2 atm; CO, 23.8 atm; H_2, 3.4 atm.

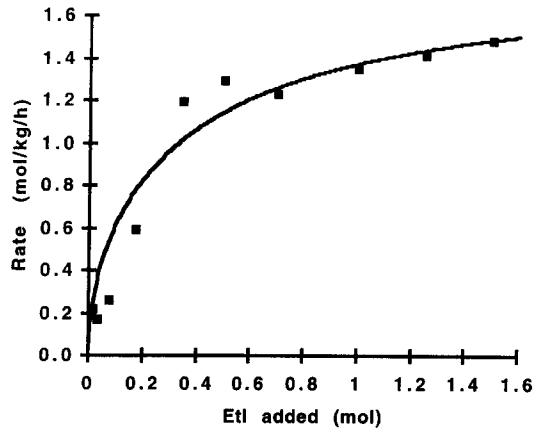

Fig. 7. Effect of *Et*I levels. Initial composition: *Et*COOH, 7.5 mol; $Mo(CO)_6$, 22 mmol; Bu_4PI, 40 mmol. Conditions: temperature, 160°C; pressures: ethylene, 27.2 atm; CO, 23.8 atm; H_2, 3.4 atm.

standing further, we found the dependence upon *Et*I (with all other variables held constant) to be consistent with the general form:

$$\text{Rate} = \frac{C_1[EtI_{added}]^{1/2}}{(C_2 + [EtI_{added}])^{1/2}} \quad (5)$$

The curve displayed in Fig. 7 fits this equation, where C_1 and C_2 have been estimated as 1.83 and 0.78, respectively. The rationale for this complex expression

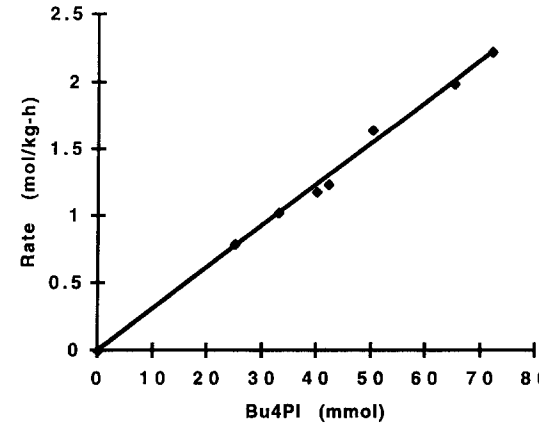

Fig. 8. Effect of $[Bu_4P]I$ levels. Initial composition: *Et*I, 0.7 mol; *Et*COOH, 7.5 mol; $Mo(CO)_6$, 22 mmol. Conditions: temperature, 160°C; pressures: ethylene, 27.2 atm; CO, 23.8 atm; H_2, 3.4 atm.

will become clearer in the next section where we will discuss the construction of the mechanism of this process.

The kinetic behavior of the iodide salt levels was much less complex. As shown in Fig. 8, the reaction is first order (r^2=0.98) with respect to the level of Bu_4PI added. The approximately 1/2 order behaviors of *Et*I and $Mo(CO)_6$ are indicative of a free radical reaction. In addition, the first order behavior of iodide indicates that it is involved in a key product generation step in the reaction sequence.

3.2.5. *Effect of temperature: determination of activation parameters*

The effect of temperature was measured between 130–170°C using identical levels of gas and catalyst components throughout the full range of temperatures. The energy of activation (E_{act}) was determined from an Arrhenius plot (Fig. 9, r^2=0.99) and was found to be 39.3 kcal mol^{-1}. Enthalpy and entropy of activation ($\Delta H^{\ddagger}$ and $\Delta S^{\ddagger}$, respectively) could be determined either from the Arrhenius plot or an Eyering plot (ln (k/T) vs. $1/T$). Although the rate orders were complex with odd dependencies upon $Mo(CO)_6$, Bu_4PI, *Et*I and CO, we determined estimated rate constants (k) for use in the Eyering plot using the following equation:

$$k = \frac{\text{Rate} \times [P_{co}]^{1.17}}{[Mo(CO)_6]^{0.62}[EtI]^{0.52}[I^-]} \quad (6)$$

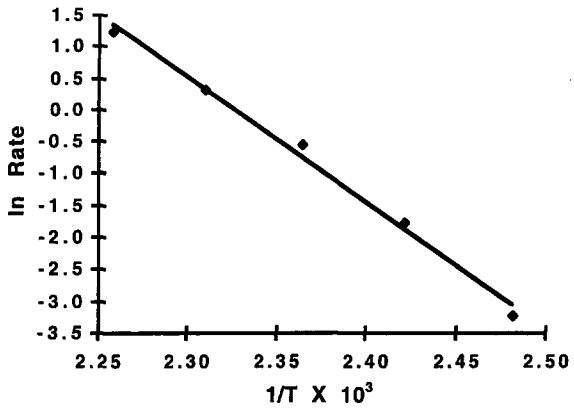

Fig. 9. Arrhenius plot. Initial composition: *Et*I, 0.7 mol; *Et*COOH, 7.5 mol; $Mo(CO)_6$, 22 mmol; Bu_4PI, 40 mmol. Pressures: ethylene, 27.2 atm; CO, 23.8 atm; H_2, 3.4 atm.

The exponential terms in Eq. (6) represent the experimentally determined rate orders for $Mo(CO)_6$, Bu_4PI, *Et*I and CO as determined from the best fit of the data obtained in the studies of the gas and catalyst component dependencies discussed in the previous section. In this way, we were able to generate an Eyering plot (Fig. 10, r^2=0.99) and subsequently determine the enthalpy of activation ($\Delta H^{\ddagger}$) and entropy of activation ($\Delta S^{\ddagger}$). From the Eyering plot, $\Delta H^{\ddagger}$ was found to be +38.4 kcal mol^{-1} and $\Delta S^{\ddagger}$ was estimated to be +40 cal mol^{-1} K^{-1} (it is important to indicate that, by keeping the CO pressure and the catalyst components constant between experiments, inaccuracies in the reaction orders used within Eq. (6) have no effect upon the measured $\Delta H^{\ddagger}$ and only negligible effect upon the magnitude of $\Delta S^{\ddagger}$. For purposes of determining the activation parameters, the density of the solution was assumed to be 1 g ml^{-1} which represents our best approximation of density at operating conditions). The raw data for this determination appear in Table 3.

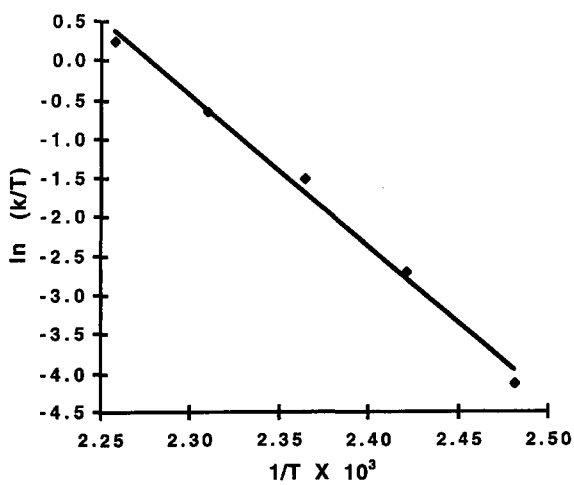

Fig. 10. Eyering plot. Initial composition: *Et*I, 0.7 mol; *Et*COOH, 7.5 mol; $Mo(CO)_6$, 22 mmol; Bu_4PI, 40 mmol. Pressures: ethylene, 27.2 atm; CO, 23.8 atm; H_2, – 3.4 atm.

These activation parameters are very significant in understanding the mechanism. The large, positive $\Delta S^{\ddagger}$ is indicative of a rate-limiting dissociative step in the process. Further, the most recent (and reliable) estimations establish the dissociation energy of the Mo–CO bond in $Mo(CO)_6$ (Eq. (7)) to be approx. 40 kcal mol^{-1} [15]. This is almost identical to our determined E_{act} and, along with the positive $\Delta S^{\ddagger}$, indicates that the rate limiting step in our process is the dissociation of CO from $Mo(CO)_6$ as displayed in Eq. (7).

$$Mo(CO)_6 \rightleftharpoons Mo(CO)_5 + CO \quad (7)$$

The experimentally determined differences in the E_{act} and $\Delta H^{\ddagger}$ are also consistent with this dissociation process. In a process which generates a mole of gas, as in Eq. (7), the expected difference between these two values would be 0.84 kcal mol^{-1} at 150°C, which coincides with our observed difference.

3.2.6. *Addition of duroquinone and other metals*

The addition of duroquinone as a free radical scavenger, generally either shuts off, or at least sig-

Table 3
Temperature dependence for the Mo catalyzed carbonylation of ethylene to propionic anhydride [a]

Temperature (°C)	Measured rate (mol K^{-1} h^{-1})	Calculated k (J mol^{-1} s^{-1})
130	0.04	6.56
140	0.17	27.9
150	0.58	95.1
160	1.39	228
170	3.49	572

[a] Initial composition: *Et*I, 0.7 mol; *Et*COOH, 7.5 mol; $Mo(CO)_6$, 22 mmol; Bu_4PI, 40 mmol. Pressures: ethylene, 27.2 atm; CO, 23.8 atm; H_2, 3.4 atm.

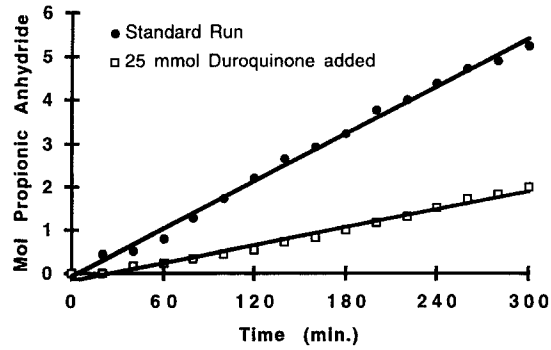

Fig. 11. Effect of duroquinone. Initial composition: *Et*I, 0.7 mol; *Et*COOH, 7.5 mol; $Mo(CO)_6$, 22 mmol; Bu_4PI, 40 mmol. Conditions: temperature, 160°C; pressures: ethylene, 27.2 atm; CO, 23.8 atm; H_2, 3.4 atm.

nificantly slows, free radical processes. As illustrated in Fig. 11, addition of 1.1 mol duroquinone (mol Mo)$^{-1}$ causes the reaction to proceed at a markedly lower rate. We initially were of the opinion that duroquinone might be slowing the reaction by acting as an oxidant for $Mo(CO)_6$. However, these fears were allayed by an in-situ infrared spectroscopic experiment in which duroquinone was added to the catalyst mixture. The Mo carbonyl spectra were virtually indistinguishable from runs in the absence of duroquinone and the Mo was clearly not oxidized to $Mo(CO)_4I_3^-$ as feared.

One interesting feature of this experiment is that duroquinone does not completely shut down the reaction. This would indicate that the rate of reaction between the initially formed radicals and the components of our catalytic system is competitive with the rate of reaction of the initially formed radicals with duroquinone. We have also observed inhibition of the Mo catalyzed ethylene carbonylation by other metals, as they may compete to scavenge radicals needed to initiate the process. For example, Ni and Fe noticeably slow the reaction and Sn almost completely inhibits the process (see Table 4).

3.2.7. *Attempted carbonylations of either methanol or benzyl alcohol derivatives*

As alluded to earlier, this catalyst is not very effective in carbonylations involving benzyl halide or MeI intermediates (i.e., carbonylation of benzyl alcohol or methanol derivatives, respectively). This observation already rules out many of the familiar

Table 4
Inhibition of ethylene carbonylation to propionic anhydride by various additives [a]

Entry	Inhibitor (mmol)	Rate (mol kg^{-1} h^{-1})
1	None	1.39
2	Duroquinone (25 mmol)	0.41
3	NiI_2 (22 mmol)	0.97
4	FeI_2(22 mmol)	0.88
5	SnI_2 (22 mmol)	0.07

[a] Initial composition: *Et*I, 0.7 mol; *Et*COOH, 7.5 mol; $Mo(CO)_6$, 22 mmol; Bu_4PI, 40 mmol. Conditions: temperature, 160°C; pressures: ethylene, 27.2 atm; CO, 23.8 atm; H_2, 3.4 atm.

mechanisms involving nucleophilic displacement of the iodide. However, studies on these substrates do provide further important insights. Studies of the stoichiometric reactions between $Mo(CO)_6$, Bu_4PBr and benzyl bromide under CO yielded toluene and bibenzyl among several products, clearly indicative of the presence of benzylic radicals, while yielding only small quantities of phenylacetate derivatives.

3.2.8. *Other significant observations*

We attempted to look at radical traps such as the 6-bromo-1-hexene and 5-bromo-1-pentene (to capture an acyl radical intermediate). Unfortunately, this catalyst is a very effective olefin isomerization catalyst and the olefins were scrambled more rapidly than carbonylation proceeded.

EPR examinations of this system are underway and appear to be more fruitful. Initial results indicate that the interaction of $Mo(CO)_6$ with *Et*I and Bu_4PI, generates a detectable organic radical and a detectable Mo based radical (defined by its diagnostic 5/2 splitting pattern). However, neither has been completely characterized to date (we are currently trying to characterize these radicals and will report on these in a separate publication).

3.3. *Mechanistic interpretation*

In assessing the mechanism, the results described in Section 3.2 provided the following general framework:

1. Based on the in situ infrared spectroscopic studies, the largely predominant Mo species in the process

is $Mo(CO)_6$ which is slowly oxidized by *Et*I to $Mo(CO)_4I_3^-$. In the presence of even small amounts of hydrogen (generated either in situ or intentionally introduced) the two species quickly reach a steady state in which $Mo(CO)_4I_3^-$ is only a minor component. $Mo(CO)_5I^-$ is generated in very minor amounts and, although initially believed to be important, now appears to be an inconsequential species in the reaction based on the kinetics.

2. The activation parameters indicated that the rate limiting step may have been the dissociation of CO from $Mo(CO)_6$.
3. The nearly 1/2 order kinetics, detection of dimeric by-products, suppression by duroquinone, and detection of (albeit still uncharacterized) EPR signals, indicated that a free radical process is operative.
4. The lack of reactivity for substrates other than olefins led us to believe that the key step in ethylene activation did not involve oxidative addition of *Et*I, since MeI and benzyl halides should be reactive under these circumstances. Most likely, the activation of ethylene involved insertion into a metal hydride species.

The key task was to develop a mechanistic proposal within the above framework which was also consistent with the complex kinetics. Classically, free radical processes are broken down into a sequence of three general portions of the reaction: initiation, chain propagation and termination (subsequent rate expressions can generally be closely approximated using the steady-state approximation). If one is familiar with the behavior of free radical systems, the kinetics, despite their complexity, provide additional insights into the events which occur within each of these portions of the reaction sequence, even before the development of a complete rate expression. Specifically:

1. The 1/2 order kinetics in *Et*I and Mo indicate that the initiation step involves a bimolecular interaction of Mo and *Et*I to ultimately form radicals.
2. The >1st inverse dependence upon CO further indicates that the initiation is inhibited by CO in both the initiation phase and in a subsequent step leading to product formation. This is consistent with proposed rate limiting initiation via a CO dissociation from $Mo(CO)_6$.
3. The predominant termination step should not involve the radicals initially generated by the interaction of Mo and *Et*I, as this would have led to either 3/2 or 1st order kinetic behavior. Instead, to be consistent with the 1/2 order behavior in the initiating species, the predominant termination step would have to involve a radical formed later in the process.
4. The 1st order kinetics in iodide and the >1st inverse order in CO indicated that there had to be a competitive reaction between iodide and CO within the chain propagating sequence. Further, since inhibition in chain propagating steps is due to chain shortening, the species formed from added CO is the most likely candidate for the predominant radical species leading to termination.
5. Ethylene addition must lie outside the transformation of initially formed radicals and the product formation step since there was no dependence upon ethylene.

These guidelines led us to propose the mechanism outlined in Scheme 1. Using the steady state approximation, the anticipated rate expression for the process was found to be:

$$\text{Rate} = \frac{k_{11}k_7^{1/2}[EtI]^{1/2}[Mo(CO)_6]^{1/2}[I^-]}{k_{18}^{1/2}[K_{m1}[P_{co}] + [EtI]]^{1/2}[K_{m2}[P_{co}] + 1]} \quad (21)$$

where $K_{m1}=k_{-7}/k_8$ and $K_{m2}=k_{-11}/k_{12}$ and the rate constants (k_i) correspond to the reaction steps in Scheme 1. This rate expression is consistent with our observations and the choice of a termination process is important. Considering the number of species we evoked in Scheme 1, there are obviously a considerable number of potential radical coupling processes that can lead to termination. However, only one, the bimolecular interaction depicted in reaction 18, leads to the correct kinetic expression. Fortuitously, the organic products expected from this coupling agree with the key minor by-products. It is probable that other radical interactions with lower reaction rates are operative in chain termination and consequently contribute to deviations in behavior from the above expression.

Several other features of the mechanistic proposal bear additional comment. Based on the kinetics, we

Initiation (Catalyst Generation/Activation)

$$Mo(CO)_6 \rightleftharpoons Mo(CO)_5 + CO \quad (7)$$

$$Mo(CO)_5 + EtI \longrightarrow \cdot Mo(CO)_5I + Et\cdot \quad (8)$$

$$\cdot Mo(CO)_5I + EtI \longrightarrow Mo(CO)_5I_2 + Et\cdot \quad (9)$$

$$Mo(CO)_6 + Et\cdot \longrightarrow \cdot Mo(EtCO)(CO)_5 \quad (10)$$

Propagation (Catalytic Process)

$$\cdot Mo(EtCO)(CO)_5 + I^- \rightleftharpoons \cdot Mo(EtCO)(CO)_4I^- + CO \quad (11)$$

$$\cdot Mo(EtCO)(CO)_4I^- \longrightarrow \cdot Mo(CO)_4^- + EtCOI \quad (12)$$

$$\cdot Mo(CO)_4^- + CO \longrightarrow \cdot Mo(CO)_5^- \quad (13)$$

$$\cdot Mo(CO)_5^- + H^+ \longrightarrow \cdot MoH(CO)_5 \quad (14)$$

$$\cdot MoH(CO)_5 + C_2H_4 \longrightarrow \cdot Mo(CO)_5Et \quad (15)$$

$$\cdot Mo(CO)_5Et + CO \longrightarrow \cdot Mo(EtCO)(CO)_5 \quad (16)$$

$$EtCOI + EtCOOH \longrightarrow (EtCO)_2O + HI \text{ (Product Formation)} \quad (17)$$

Termination (Catalyst Deactivation)

$$2 \cdot Mo(EtCO)(CO)_5 \xrightarrow[2\,CO]{} EtCOCOEt + 2\,Mo(CO)_6 \quad (18)$$

Catalyst Regeneration (Reduction of Mo(II) by hydrogen)

$$Mo(CO)_5I_2 + I^- \longrightarrow Mo(CO)_4I_3^- \text{ (observed)} \quad (19)$$

$$Mo(CO)_4I_3^- + H_2 + CO \longrightarrow 2HI + Mo(CO)_5I^- \quad (20)$$

$$Mo(CO)_6 + I^- \rightleftharpoons Mo(CO)_5I^- + CO \quad (4)$$

Scheme 1. Proposed mechanism for the generation of propionic anhydride from ethylene, CO and propionic acid.

can obtain some additional insight into the radical generation steps. We already established that the process proceeds via a rate limiting CO dissociation as the initial step. However, contrary to earlier investigations of the interaction of benzyl bromide with $(dmpe)_2Mo(CO)_2$ (dmpe=$Me_2PCH_2CH_2PMe_2$) [16,17] where an outer sphere electron transfer seemed likely, this dissociation would infer that the initial interaction of *Et*I with Mo (reaction 8) proceeds via an inner sphere process.

Further, the small halide effect would usually indicate that the process represented by reaction 8 is an electron transfer process as alluded to earlier [10]. However, some caution needs to be exercised in interpreting this halide effect since the half order behavior associated with reaction 8 serves to dampen any halide effect. Further complicating the interpretation of the halide effect are contributions of reactions 11 and 12, both of which enter the rate expression and may influence the magnitude of the halide effect. Of particular concern is the potential effect of the halide on the crucial equilibrium expressed by reaction 11 where the halide may be very important. Therefore, although the halide effect should still be interpreted to indicate that this is an inner sphere, electron transfer process, we cannot completely rule out other potential inner sphere, one-electron processes, such as halogen atom abstraction (see Ref. [18] for a review of one electron inner sphere processes). The subsequent formation of a second ethyl radical by the interaction of the $17e^-$, $[\cdot Mo(CO)_5I]$, with *Et*I reaction 9 would be expected to be fast.

An inner sphere process would also explain the inhibition of the reaction when either methanol or water are present at high levels. In the presence of large quantities of methanol or water, it is likely that these nucleophiles will inhibit the reaction by competing with *Et*I for the vacant site on $Mo(CO)_5$.

The species we evoke in the initiation process are reasonable. Whereas [·Mo(CO)$_5$I] is not known, its dimer has been synthesized [19] and the Cr analog is a well-known, stable, free-radical metal species (for examples, see Refs. [20,21]). The seven coordinate Mo(CO)$_5$I$_2$ is not observed, but its iodide displacement product, Mo(CO)$_4$I$_3^-$, is both known and observed within the process (vide infra). The species, [·Mo(*Et*CO)(CO)$_5$], generated in the final reaction of our initiation sequence reaction 10 is, to our knowledge, unknown in the literature. However, metal species are known to be good radical traps and their formation is a rational consequence of the interaction of ethyl radical with the predominant Mo species, Mo(CO)$_6$.

The generation of the 17e$^-$ species, [·Mo(*Et*CO)(CO)$_5$], is pivotal in our proposal and this species represents the predominant radical present in the process at any given time. (As we already indicated, termination by a bimolecular reaction of this intermediate with itself is the only process we have found to be consistent with the kinetics.) Although the specific species, [·Mo(*Et*CO)(CO)$_5$], is unknown, the literature regarding 17e$^-$ Cr group species is extensive and these complexes are characterized by rapid ligand exchanges, rapid oxidative addition/ reductive elimination processes, and rapid dimerization. (For descriptions of the chemistry of 17e$^-$ Cr group species see [10,22], and the numerous references cited therein.) The ability to undergo rapid ligand exchange is particularly important within our process. Whereas Mo(0) and Mo(+2) are generally slow to undergo ligand exchange, a process usually critical to catalysis with olefins, the 17e$^-$ Mo species undergo rapid ligand exchange, allowing ethylene and iodide to rapidly coordinate with the catalyst at critical junctures during chain propagation.

As indicated earlier, the specific steps within our propagation steps were dictated by kinetics. As regards the individual species, only one of the species evoked in the propagation sequence is known. [·Mo(CO)$_5^-$] has been identified a number of times in the literature (see Ref. [23] for the earliest example). Unless frozen in a matrix, it has a lifetime of only a few seconds. The dimers, Mo$_2$(CO)$_{10}^{2-}$ and (μ-*H*)Mo$_2$(CO)$_{10}^-$ (resulting from coupling combinations of [·Mo(CO)$_5^-$] and [·HMo(CO)$_5$]) are well established, but neither species is observed in the process (see Refs. [24,25] for earliest examples).

As indicated by kinetics, the predominant chain termination process most likely involved a bimolecular interaction of the pivotal intermediate, [·Mo(*Et*CO)(CO)$_5$]. Unfortunately, beyond this insight, the information to date does not give any additional indication of the exact mechanism. Based on the propensity of these 17e$^-$ Mo species to dimerize, one would be tempted to evoke a dimerization to form [Mo(*Et*CO)(CO)$_5$]$_2$ with subsequent intramolecular elimination of *Et*COCO*Et*. However, in the absence of any additional data, the possibility that the reaction may proceed through any of a number of alternative bimolecular processes, including metal to metal electron transfer to generate Mo(0) and Mo(+2) species, cannot be excluded.

4. Conclusion

The carbonylation of olefins, particularly ethylene, with a halide promoted Mo catalyst represents the first efficient carbonylation process using a Cr group metal as the active catalytic species. Detailed mechanistic examinations indicate that the reaction proceeds via a free radical pathway which is initiated by a rate limiting dissociation of CO from Mo(CO)$_6$. This initial dissociation is followed by a subsequent radical generation step involving the interaction of *Et*I with the coordinatively unsaturated species, Mo(CO)$_5$, to ultimately form ethyl radicals. It would be expected that the resultant ethyl radicals would be captured by Mo(CO)$_6$ to form the pivotal complex [·Mo(*Et*CO)(CO)$_5$], which allows entry into a chain propagation sequence which is responsible for catalysis. The addition of iodide to the complex, [·Mo(*Et*CO)(CO)$_5$], generates *Et*COI, a precursor to the propionate derivatives and allows eventual regeneration of the pivotal complex, [·Mo(*Et*CO)(CO)$_5$].

The precise propionate derivative obtained is determined by the nature of the nucleophilic component. Care must be taken in generating propionate esters and propionic acid. If present in too large a quantity, the nucleophilic component (an alcohol or water, respectively) can effectively inhibit the initiation of the process by competing with *Et*I for the vacant coordination site in Mo(CO)$_5$.

Acknowledgements

We wish to thank the US Department of Energy and Eastman Chemical Company for their joint support of this work under US Department of Energy Contract No. DE-AC22-94PC94065 and Norma L. Buchanan for technical assistance in the high-pressure infrared spectroscopic measurements.

References

[1] U.R. Samel, W. Kohler, A.O. Gamer and U. Keuser, Propionic Acid and Derivatives, in Ullman's Encyclopedia of Industrial Chemistry, 5th edn., Vol. A22, VCH Publishers, New York, NY, 1993, p. 223.
[2] W. Bertleff, Carbonylation, in: Ullman's Encyclopedia of Industrial Chemistry, 5th edn., Vol. A5, VCH Publishers, New York, NY, 1986, p. 223.
[3] P. Pino, F. Piacenti and M. Bianchi, in: Organic Syntheses via Metal Carbonyls, 1st edn., Wender and P. Pino, Vol. 2, Wiley, New York, NY, 1977, pp. 233–296.
[4] A. Mullen, in J. Falbe (Ed.), New Syntheses with Carbon Monoxide, Springer, Berlin, 1980, pp. 275–286.
[5] H.M. Colquhoun, D.J. Thompson and M.V. Twigg, Carbonylation-Direct Synthesis of Carbonyl Compounds, Plenum Press, New York, NY, 1991, pp. 102–106; 119–130.
[6] D. Forster, A. Hershman and D.E. Morris, Catalysis Rev.-Sci. Eng., 23 (1981) 89.
[7] M. Imbeaux, H. Mestdagh, K. Moughamir and C. Rolando, J. Chem. Soc. Chem. Comm., (1992) 1678–1679.
[8] B.M. Lichstein, US Patent No. 3790607, 1974.
[9] J.R. Zoeller and C.J. Ackerman, J. Org. Chem., 55 (1990) 1354.
[10] T.A. Huber, D.H. Macartney and M.C. Baird, Organometals, 14 (1995) 592.
[11] R.B. King, Inorg. Chem., 3 (1964) 1039.
[12] M.C. Ganorkar and M.H.B. Stiddard, J. Chem. Soc., (1965) 3494.
[13] E.W. Abel, I.S. Butler and J.G. Reid, J. Chem. Soc., (1963) 2068.
[14] E.W. Abel, M.A. Bennett and G. Wilkinson, Chem. Ind., (1960) 442.
[15] A.W. Ehlers and G. Frenking, J. Chem. Soc., Chem. Comm., (1993) 1709; J. Am. Chem. Soc., 116 (1994) 1514.
[16] J.A. Conner and P.I. Riley, J. Chem. Soc., Dalton Trans., (1979) 1318.
[17] J.A. Conner and P.I. Riley, J. Chem. Soc. Chem. Comm., (1976) 634.
[18] J.P. Collman, L.S. Hegedus, J.R. Norton and R.G. Finke, Principles and Applications of Organotransition Metal Chemistry, University Science Books, Mill Valley, CA, 1987, Chapter 5.
[19] C. Schmid, R. Boese and E. Welz, Chem. Ber., 108 (1975) 260.
[20] H. Behrens, R. Schwab and D. Hermann, Z. Naturforsch., Teil B, 21 (1966) 590.
[21] H. Behrens and R. Schwab, Z. Naturforsch., Teil B, 19 (1964) 768.
[22] S.L. Scott, J.H. Espenson and A. Bakac, Organometals, 12 (1993) 1044.
[23] C.J. Pickett and D. Pletcher, J. Chem. Soc., Dalton Trans., (1976) 749.
[24] C.J. Pickett and D. Pletcher, J. Chem. Soc., Dalton Trans., (1975) 879.
[25] R.G. Hayter, J. Am. Chem. Soc., 88 (1966) 4376.